Bayesian approach to patient-tailored vectorcardiography

Bayesian Approach to Patient-Tailored Vectorcardiography

Rik Vullings*, Chris H. L. Peters, Iman Mossavat, S. Guid Oei, and Jan W. M. Bergmans, *Senior Member, IEEE*

***Abstract*—For assessment of specific cardiac pathologies, vectorcardiography is generally considered superior with respect to electrocardiography. Existing vectorcardiography methods operate by calculating the vectorcardiogram (VCG) as a fixed linear combination of ECG signals. These methods, with the inverse Dower matrix method the current standard, are therefore not flexible with respect to different body compositions and geometries. Hence, they cannot be applied with accuracy on patients that do not conform to the fixed standard. Typical examples of such patients are obese patients or fetuses. For the latter category, when recording the fetal ECG from the maternal abdomen the distance of the fetal heart with respect to the electrodes is unknown. Consequently, also the signal attenuation/transformation per electrode is not known. In this paper, a Bayesian method is developed that estimates the VCG and, to some extent, also the signal attenuation in multichannel ECG recordings from either the adult 12-lead ECG or the maternal abdomen. This is done by determining for which VCG and signal attenuation the joint probability over both these variables is maximal given the observed ECG signals. The underlying joint probability distribution is determined by assuming the ECG signals to originate from scaled VCG projections and additive noise. With this method, a VCG, tailored to each specific patient, is determined. The method is compared to the inverse Dower matrix method by applying both methods on standard 12-lead ECG recordings and evaluating the performance in predicting ECG signals from the determined VCG. In addition, to model nonstandard patients, the 12-lead ECG signals are randomly scaled and, once more, the performance in predicting ECG signals from the VCG is compared between both methods. Finally, both methods are also compared on fetal ECG signals that are obtained from the maternal abdomen. For patients conforming to the standard, both methods perform similarly, with the developed method performing marginally better. For scaled ECG signals and fetal ECG signals, the developed method significantly outperforms the inverse Dower matrix method.**

***Index Terms*—Cardiac electrical imaging, fetal electrocardiography, fetal monitoring, medical signal processing, vectorcardiography.**

Manuscript received July 16, 2009; revised August 31, 2009 and September 8, 2009. First published October 20, 2009; current version published February 17, 2010. This work was supported by the Dutch Technology Foundation STW. *Asterisk indicates corresponding author.*

*R. Vullings is with the Department of Electrical Engineering, Eindhoven University of Technology, Eindhoven 5600 MB, The Netherlands (e-mail: r.vullings@tue.nl).

C. H. L. Peters is with the Department of Clinical Physics, Amphia Hospital, Breda 4818 CK, The Netherlands, and also with Eindhoven University of Technology, Eindhoven 5600 MB, The Netherlands (e-mail: cpeters@amphia.nl).

I. Mossavat and J. W. M. Bergmans are with the Department of Electrical Engineering, Eindhoven University of Technology, Eindhoven 5600 MB, The Netherlands (e-mail: s.i.mossavat@tue.nl; j.w.m.bergmans@tue.nl).

S. G. Oei is with the Department of Obstetrics and Gynecology, Máxima Medical Center, Veldhoven 5500 MB, The Netherlands, and also with the Department of Electrical Engineering, Eindhoven University of Technology, Eindhoven 5600 MB, The Netherlands (e-mail: g.oei@mmc.nl).

Digital Object Identifier 10.1109/TBME.2009.2033664

I. Introduction

CARDIAC contractions originate from the propagation of an action potential through the cardiac tissues. The front of the propagating action potential causes the occurrence of numerous electrical dipoles. By superimposing these electrical dipoles at each point in time, the electrical activity of the heart can be modeled as a single electrical field vector, originating in the heart, that varies in both amplitude and orientation over time [1], [2]. The time path of this electrical field vector during a single cardiac contraction is referred to as the vectorcardiogram (VCG). The ECG recorded at the cutaneous surface can be viewed as the potential caused by this electrical field vector, and therefore, depends on both the distance between the recording electrode and the heart and on the conductive properties of the intermediate tissues. It has to be noted here that in this dipole model, the electrical field vector (and with that the VCG) is reported to only describe between 70% and 95% of the power of the ECG [1], [3], [4]. The remaining 5%–30% of the ECG originates from insufficiencies in the dipole model such as the inclusion nondipolar components [5] and movement of the dipole origin [6].

The problem of improving the dipole model, with the goal of completely imaging and visualizing the electrical activity of the heart, has been addressed by researchers in the field of cardiac electrical imaging [7]–[9]. However, as nearly all the proposed methods for imaging the electrical activity are based on body surface potential maps (BSPMs), i.e., lead systems consisting of a relatively large number of electrodes [10], for reasons of workability none of these methods has made its way into clinical practice. Clinicians generally prefer to use the standard 12-lead ECG for assessing the condition of the heart, in spite of the diagnostic inferiority of the 12-lead ECG with respect to BSPM.

With recent improvements in (wireless) data acquisition technology, the interest in ambulatory ECG monitoring is rapidly increasing. In order to increase patient comfort and reduce bandwidth requirements, the use of as few ECG leads as possible is preferred. However, as mentioned earlier, clinicians are accustomed to using the 12-lead ECG, theoretically implying that all 12 ECG leads need to be recorded and subsequently transmitted. By determining the VCG from fewer than 12 leads and using this VCG to predict the remaining leads, nevertheless, the problem of patient discomfort can be overcome. In addition, for assessing specific cardiac pathologies like right ventricular hypertrophy and myocardial infarcts, direct analysis of the VCG is considered to be superior with respect to 12-lead electrocardiography [11].

As mentioned previously, the relation between the ECG at the cutaneous surface and the VCG depends on the distance between the heart and the electrodes and the conductive properties of the intermediate tissues. The currently most widely used method to determine the VCG from a ECG recording, referred to as the inverse Dower method [12], accounts for both this distance and conductive properties. It entails a fixed, numerical description of a matrix that maps the VCG onto the 12-lead ECG. Due to this fixed numerical description, however, it assumes the same geometry and conductive properties for all patients. Consequently, it cannot provide accurate VCGs for patients that do not conform to the assumed conduction characteristics, such as patients that suffer from severe obesity. This category of patients has an increased risk of cardiac failure [13], and is therefore, in more need of VCG examination than "standard" patients.

When determining the VCG of the fetus through ECG recordings on the maternal abdomen, the problem of patients not conforming to the model is even more evident [14]. Not only does the position of the fetal heart with respect to the abdominal electrodes vary between patients, but also do, among other variations, the amount of amniotic fluid, placental position, and abdominal fat differ from one pregnant woman to the other. Hence, for determining the fetal VCG, the inverse Dower matrix can only contain information on the electrode positions and not on the unknown heart–electrode distance and conduction properties. These conduction properties are unknown as, in contrast to the regular VCG, few models on the fetal signal propagation exist and the models that do exist cannot account for all possible positions of the fetal heart [15]. Even so, determining the fetal VCG can have significant value in fetal health monitoring. Changes in orientation of the QRS loop, for instance, can be an indication of fetal movement [16], while fetal ECG analysis—which can provide information on fetal oxygenation [17]—is facilitated by projecting the VCG onto leads that are familiar to physicians [18]. In addition, early-stage diagnosis of fetal congenital cardiac disease might in future become treatable and is facilitated by vectorcardiography, i.e, by projecting the VCG onto the leads used in standard 12-lead ECG analysis.

The common problem in these VCG applications is the lack of a way to account for variations in the composition and geometry of the tissues between the heart and cutaneous surface, leading to inaccurate VCG estimates for patients that do not conform to the standard. Naturally, by performing MRI or ultrasound analysis prior to the ECG recording, the geometry of the intermediate tissues can be estimated and accounted for. However, particularly in case of the fetal VCG, the geometry is not expected to remain the same throughout the recording. Moreover, for ambulatory applications the use of MRI or ultrasound is not practical. To nevertheless account for variations in the composition and geometry of intermediate tissues, in this paper a method is developed for patient-tailored vectorcardiography (PTV), i.e., for determination of the VCG from multilead ECG recordings considering the geometrical and compositional variations. For quantitative evaluation, the method is applied to both nonstandard adult ECG and fetal ECG recordings.

The method uses Bayesian probability theory to determine the joint probability distribution for both the VCG and a scaling matrix that models the attenuation at each recording site, given the recorded ECG. This probability distribution is based on a simplified model of the relation between the VCG and ECG. This model stipulates that the ECG at each recording site is generated by the projection of the VCG onto the corresponding ECG lead vector. To account for attenuation effects, each projected VCG is scaled by an *a priori* unknown scaling parameter. Inaccuracies in the model and noise in the ECG are assumed to originate from a Gaussian distribution. The optimal VCG estimate, in the sense of the maximum *a posteriori* (MAP) solution, is obtained from the joint probability distribution by means of an approximate inference technique referred to as variational inference [19].

Besides analysis of the contour and orientation of the QRS loop, the VCG is mainly used for predicting the shape of ECG signals that are not physically recorded. This provides a way for evaluating the developed method, namely, the method can be evaluated by recording separate reference ECG signals and comparing these to the prediction of these signals from the VCG. To quantitatively evaluate the performance of the developed method on nonstandard adult patients, this evaluation approach is applied on randomly scaled adult ECG signals.

To recapitulate, the developed method for vectorcardiography models the conductive properties of the tissues between cutaneous electrodes and the heart and estimates the parameters of this model to obtain a patient-tailored estimate of the VCG. Applications of this method include improved assessment of the adult VCG, in particular for nonaverage patients, and assessment of the fetal VCG from noninvasive recordings. As a basis of reference for the developed method in Section II, the inverse Dower matrix method is discussed briefly. In Section III, the developed method is presented. Section IV discusses the acquisition of the data and the evaluation of the method, while in Section V, the results are presented. Finally, in Section VI, these results are discussed and conclusions are drawn.

II. Inverse Dower Matrix for Vectorcardiography

The Dower matrix was introduced by Dower *et al.* [12] and describes the matrix that maps the VCG onto the 12-lead ECG signals, taking into account standardized electrode positions and nonlinear signal attenuation effects. Even though the Dower matrix does not account for interpatient variability, in practice the resulting VCG estimate is clinically useful [12].

By defining $\mathbf{V}$ as the $[N \times T]$ ECG matrix and $\mathbf{D}$ as the $[N \times 3]$ Dower matrix, the relation between these matrices can be described by

$$\mathbf{V} = \mathbf{DS} + \mathbf{H} \tag{1}$$

with $\mathbf{S}$ the $[3 \times T]$ VCG matrix and $\mathbf{H}$ a $[N \times T]$ noise matrix with zero-mean Gaussian distribution for each row.

The model of (1) is significantly simplified. In reality, not only is the noise expected to be non-Gaussian, including nondipolar components of the electrical activity of the heart, but also do boundary effects and inhomogeneities of the conductive medium play a significant role. To account for these effects, the fixed numerical Dower matrix $\mathbf{D}$ is defined in such a way

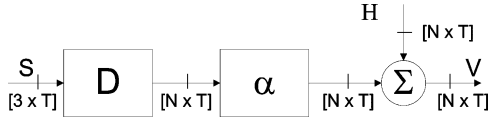

Fig. 1. Schematic overview of the model describing the relation between the VCG and the ECG. The VCG is projected onto the matrix $\mathbf{D}$ containing electrode positions and subsequently scaled by the diagonal matrix α to model attenuation effects. Imperfections in this model and additional noise are described by the noise matrix $\mathbf{H}$.

that is does not only consider the electrode positions with respect to one another, but also considers the boundary and conductivity effects to some extent. More in particular, for an infinite uniform medium the mapping matrix between the VCG and ECG would only contain electrode positions. Any difference between the Dower matrix and electrode positions has, thus, been intended to account for boundary effects and tissue inhomogeneities.

In this simplified model of (1), the optimal VCG estimate $\hat{\mathbf{S}}_{\mathrm{Dower}}$ can be assessed as the maximum-likelihood (ML) solution

$$\hat{\mathbf{S}}_{\mathrm{Dower}} = \left(\mathbf{D}^T\mathbf{D}\right)^{-1}\mathbf{D}^T\mathbf{V} = \mathbf{D}^{\dagger}\mathbf{V} \tag{2}$$

with $\mathbf{D}^{\dagger}$ the Moore–Penrose pseudoinverse [20], [21] of the Dower matrix.

III. Bayesian Vectorcardiography

A. Interpatient ECG Variability

For each patient the position of the heart with respect to the cutaneous electrodes and the conductive properties of the intermediate tissues is different. Because of its fixed numerical nature, the Dower matrix cannot account for any of these differences. However, although the matrix that maps the VCG onto the ECG is expected to vary in a nonlinear way as a function of interpatient differences in geometry and conductivity, by assuming an individual scaling for each ECG signal, these nonlinear variations can be approximated to a first order as (see also Fig. 1)

$$\mathbf{V} = \boldsymbol{\alpha}\mathbf{D}\mathbf{S} + \mathbf{H}. \tag{3}$$

Here, $\boldsymbol{\alpha}$ is an $[N \times N]$ diagonal scaling matrix of which the diagonal elements α_i represent the linear scaling of the ECG signals $\vec{V}_i$ and $\mathbf{H}$ is a $[N \times T]$ matrix representing noise in the ECG signals. The reason that $\boldsymbol{\alpha}$ is taken a diagonal scaling matrix follows directly from the assumption of individual scaling for each ECG signal. Namely, the ith row of the matrix $\mathbf{V}$ represents the projection of the VCG $\mathbf{S}$ onto the ith row of $\mathbf{D}$, scaled with a constant α_i. The matrix representation of this scaling yields a matrix with α_i on the diagonal and zeros elsewhere. The reason for keeping the matrix multiplications $\mathbf{D}$ and $\boldsymbol{\alpha}$ separated in this model is the fact that the matrix $\mathbf{D}$ is assumed known, i.e., the Dower matrix, while the elements of $\boldsymbol{\alpha}$ are as yet unknown model parameters.

Since both $\mathbf{S}$, $\boldsymbol{\alpha}$, and $\mathbf{H}$ are unknown, the VCG $\mathbf{S}$ cannot be readily assessed from $\mathbf{V}$. However, by employing a statistical analysis, the VCG can be estimated, given only the ECG $\mathbf{V}$, Dower matrix $\mathbf{D}$, and noise variance $\boldsymbol{\Sigma}$ plus some assumptions on statistical independencies and noise characteristics, which are made explicit in Section III-B.

B. Statistical Analysis

Assuming the noise $\mathbf{H}$ to have a Gaussian probability distribution with zero mean and variance $\boldsymbol{\Sigma}$ and using Bayes' theorem [22], the joint probability distribution of $\mathbf{S}$ and $\boldsymbol{\alpha}$, given $\mathbf{V}$, $\mathbf{D}$, and $\boldsymbol{\Sigma}$ obeys

$$p\left(\mathbf{S},\boldsymbol{\alpha}\,|\mathbf{V},\mathbf{D},\boldsymbol{\Sigma}\right) = p\left(\mathbf{S},\boldsymbol{\alpha}\,|\mathbf{D},\boldsymbol{\Sigma}\right)\frac{p\left(\mathbf{V}\,|\mathbf{D},\mathbf{S},\boldsymbol{\alpha},\boldsymbol{\Sigma}\right)}{p\left(\mathbf{V}\,|\mathbf{D},\boldsymbol{\Sigma}\right)}. \tag{4}$$

The reason for assuming the noise to have a zero-mean Gaussian distribution is similar as for (1); boundary effects and tissue inhomogeneities are taken to be accounted for by the definition of the Dower matrix $\mathbf{D}$. In addition, interpatient variability in these boundary effects and inhomogeneities are approximated by the linear scaling $\boldsymbol{\alpha}$. The reason for using this simplified model of the interpatient variability and noise is to yield an analytical tractable solution for the VCG estimation problem.

Considering the evidence $p(\mathbf{V}|\mathbf{D},\boldsymbol{\Sigma})$ in (4) a normalization term, assuming $\boldsymbol{\alpha}$ and $\mathbf{S}$ *a priori* statistically independent, and assuming no prior knowledge on $\mathbf{S}$, hence taking $p(\mathbf{S}|\mathbf{D},\boldsymbol{\Sigma})$ to be a uniform distribution, (4) can be rewritten as

$$p\left(\mathbf{S},\boldsymbol{\alpha}\,|\mathbf{V},\mathbf{D},\boldsymbol{\Sigma}\right) \propto p\left(\boldsymbol{\alpha}\,|\mathbf{D},\boldsymbol{\Sigma}\right)p\left(\mathbf{V}\,|\mathbf{D},\mathbf{S},\boldsymbol{\alpha},\boldsymbol{\Sigma}\right). \tag{5}$$

The terms on the right-hand side of (5) are referred to as the prior probability distribution and likelihood, respectively. The assumption of $\boldsymbol{\alpha}$ and $\mathbf{S}$ to be *a priori* statistically independent can, intuitively, be explained by the fact that $\mathbf{S}$ is affected by changes in the electrical activity of the heart while $\boldsymbol{\alpha}$ is only affected by changes in the propagation path between the heart and the cutaneous surface.

As mentioned previously, $\boldsymbol{\alpha}$ represents a first-order approximation of the variations in the ECG caused by interpatient differences in boundary effects and tissue inhomogeneities. As a result, the elements of $\boldsymbol{\alpha}$ are, among other factors, related to the distance between heart and electrodes. With information on the distance between the heart and electrode i also providing information on the distance between the heart and electrode k, the elements α_i are mutually dependent. For reasons of mathematical simplicity, however, the elements of $\boldsymbol{\alpha}$ are assumed to be statistically independent [23], and thus, the prior probability distribution can be expressed as

$$p\left(\boldsymbol{\alpha}\,|\mathbf{D},\boldsymbol{\Sigma}\right) = \prod_i p\left(\alpha_i\,|\mathbf{D},\boldsymbol{\Sigma}\right). \tag{6}$$

The probability distribution for each of the individual scaling elements, $p(\alpha_i|\mathbf{D},\boldsymbol{\Sigma})$, can be defined based on available models of torso geometry and conductivity [24], [25]. This would, however, lead to a mathematically complex prior distribution. To simplify the final algorithm, the prior distribution is chosen uniform yielding no prior information on $\boldsymbol{\alpha}$

$$p\left(\boldsymbol{\alpha}\,|\mathbf{D},\boldsymbol{\Sigma}\right) = \text{constant}. \tag{7}$$

The impact of these physically unjustified—but mathematically simplifying—assumptions, i.e., mutual independency of the elements of $\boldsymbol{\alpha}$ and an uniform prior probability distribution for

$p(\boldsymbol{\alpha}|\mathbf{D},\boldsymbol{\Sigma})$, on the performance of the developed PTV method is discussed later on in Section VI.

As mentioned previously, the noise $\mathbf{H}$ is assumed to have a zero-mean Gaussian distribution with variance $\boldsymbol{\Sigma}$. Combining this with the model of (3) and the assumption that the rows of both $\mathbf{V}$ and $\mathbf{H}$ are statistically independent, the likelihood is given by

$$p\left(\mathbf{V}\,|\mathbf{D},\mathbf{S},\boldsymbol{\alpha},\boldsymbol{\Sigma}\right) = \prod_i \exp\left[-\frac{1}{2\sigma_i}\left(\vec{V}_i-\alpha_i\vec{D}_i\mathbf{S}\right)\left(\vec{V}_i-\alpha_i\vec{D}_i\mathbf{S}\right)^T\right] \quad (8)$$

where σ_i is the variance of the ith row of $\mathbf{H}$. Moreover, $\vec{V}_i$ is a time vector describing the ECG signal recorded at position $\vec{D}_i$, so that $\vec{V}_i$ is a $[1\times T]$ vector and $\vec{D}_i$ is a $[1\times 3]$ vector.

The statistical independence between the rows of $\mathbf{V}$ is justified by applying d-separation [19] on the likelihood. Intuitively, this independence can be explained by the fact that for given $\mathbf{D}$, $\mathbf{S}$, $\boldsymbol{\alpha}$, and $\boldsymbol{\Sigma}$, variations in one ECG signal do not affect any of the other ECG signals. More precisely, although the ECG signal changes, none of the variables $\mathbf{D}$, $\mathbf{S}$, $\boldsymbol{\alpha}$, and $\boldsymbol{\Sigma}$ change (as they are given), hence not affecting the other ECG signals. The assumption on statistical independence between the rows of $\mathbf{H}$ is justified analogously.

Substituting (7) and (8) into (5) yields the joint posterior probability distribution for $\mathbf{S}$ and $\boldsymbol{\alpha}$

$$\begin{aligned} p\left(\mathbf{S},\boldsymbol{\alpha}\,|\mathbf{V},\mathbf{D},\boldsymbol{\Sigma}\right) &\propto \prod_i \exp\left[-\frac{1}{2\sigma_i}(\vec{V}_i-\alpha_i\vec{D}_i\mathbf{S})(\vec{V}_i-\alpha_i\vec{D}_i\mathbf{S})^T\right] \\ &= \exp\left[-\sum_i \frac{1}{2\sigma_i}(\vec{V}_i-\alpha_i\vec{D}_i\mathbf{S})(\vec{V}_i-\alpha_i\vec{D}_i\mathbf{S})^T\right]. \end{aligned} \quad (9)$$

C. Variational Inference on VCG

Although the MAP solution for the VCG, which, in this case, is equivalent to the ML solution, can be assessed by integrating (9) over $\boldsymbol{\alpha}$ and determining for which $\mathbf{S}$ the resulting probability distribution is maximal, the required integral is impossible to evaluate analytically. However, by employing variational inference [19], in factorized form also known as mean field theory [26], the MAP solution for the VCG can be approximated.

In variational inference, the posterior probability distribution $p(\mathbf{S},\boldsymbol{\alpha}|\mathbf{V},\mathbf{D},\boldsymbol{\sigma})$ is approximated by the variational distribution $q(\mathbf{S},\boldsymbol{\alpha})$

$$p\left(\mathbf{S},\boldsymbol{\alpha}\,|\mathbf{V},\mathbf{D},\boldsymbol{\sigma}\right) \approx q\left(\mathbf{S},\boldsymbol{\alpha}\right). \quad (10)$$

The goal of variational inference is now to restrict the family of possible distributions $q(\mathbf{S},\boldsymbol{\alpha})$ sufficiently that it comprises only tractable solutions, while at the same time allowing it to be sufficiently rich and flexible to obtain a good approximation to the true posterior probability distribution.

A way of restricting the family of distributions is by assuming it to factorize into

$$q\left(\mathbf{S},\boldsymbol{\alpha}\right) = q_{\mathbf{S}}\left(\mathbf{S}\right)\prod_j q_{\alpha_j}\left(\alpha_j\right). \quad (11)$$

Substituting the factorized probability distributions from (11) into a lower bound for the true posterior, provided and discussed extensively in [19], results in an expression for the optimal solutions $q^*_{\mathbf{S}}(\mathbf{S})$ and $q^*_{\boldsymbol{\alpha}}(\boldsymbol{\alpha})$ [19]

$$\ln q^*_{\mathbf{S}}\left(\mathbf{S}\right) = \mathbf{E}_{\boldsymbol{\alpha}}\left[\ln p\left(\mathbf{V},\mathbf{S},\boldsymbol{\alpha}\,|\mathbf{D},\boldsymbol{\Sigma}\right)\right] + \text{constant} \quad (12)$$

$$\ln q^*_{\boldsymbol{\alpha}}\left(\boldsymbol{\alpha}\right) = \mathbf{E}_{\mathbf{S}}\left[\ln p\left(\mathbf{V},\mathbf{S},\boldsymbol{\alpha}\,|\mathbf{D},\boldsymbol{\Sigma}\right)\right] + \text{constant}. \quad (13)$$

Here, $\mathbf{E}_y[x]$ denotes the expected value of x with respect to the probability distribution $q(y)$.

Assuming a Gaussian distribution for $q_{\alpha_j} = \mathcal{N}(\alpha_j|\mu_j,\beta_j)$ with mean μ_j and variance β_j, the optimal solution for the VCG $\mathbf{S}$ can be evaluated as

$$\begin{aligned} \ln q^*_{\mathbf{S}}\left(\mathbf{S}\right) &= \int\prod_j \mathcal{N}\left(\alpha_j\,|\mu_j,\beta_j\right)\ln p\left(\mathbf{S},\boldsymbol{\alpha}\,|\mathbf{V},\mathbf{D},\boldsymbol{\Sigma}\right)\mathrm{d}\alpha_j \\ &\quad + \text{constant} \\ &= -\sum_i\left\{\frac{1}{2\sigma_i}(\vec{D}_i\mathbf{S})(\vec{D}_i\mathbf{S})^T(\beta_i+\mu_i^2)\right. \\ &\quad \left. - \vec{D}_i\mathbf{S}\sigma_i^{-1}\vec{V}_i^T\mu_i\right\} + \text{constant}. \end{aligned} \quad (14)$$

Since the term on the right-hand side of (14) is quadratic with respect to $\mathbf{S}$, $q^*_{\mathbf{S}}(\mathbf{S})$ is a Gaussian distribution. For reasons of convenience, this distribution is expressed with respect to $\vec{D}_i\mathbf{S}$. From (14), it follows that this distribution has mean $\vec{\nu}_i$ and variance Σ_i given by

$$\vec{\nu}_i = \frac{\mu_i}{\beta_i+\mu_i^2}\vec{V}_i \qquad \text{and} \qquad \Sigma_i = \frac{\sigma_i}{\beta_i+\mu_i^2}. \quad (15)$$

Substituting this result into (13) gives, analogous to (14)

$$\begin{aligned} &\ln q^*_{\boldsymbol{\alpha}}\left(\boldsymbol{\alpha}\right) \\ &= -\sum_i\left\{\frac{\alpha_i^2}{2\sigma_i}\left(\Sigma_i+\vec{\nu}_i\vec{\nu}_i^T\right) - \frac{\alpha_i}{\sigma_i}\vec{\nu}_i\vec{V}_i^T\right\} + \text{constant} \end{aligned} \quad (16)$$

which reflects a Gaussian distribution for $q^*_{\boldsymbol{\alpha}}(\boldsymbol{\alpha})$ as well, with mean μ_i and variance β_i given by

$$\mu_i = \frac{\vec{\nu}_i\vec{V}_i^T}{\Sigma_i+\vec{\nu}_i\vec{\nu}_i^T} \qquad \text{and} \qquad \beta_i = \frac{\sigma_i}{\Sigma_i+\vec{\nu}_i\vec{\nu}_i^T}. \quad (17)$$

Implementing (15) and (17) into an iterative procedure, an estimate for $\vec{D}_i\mathbf{S}$ can be determined. Convergence of this iteration scheme is ensured by the convexity of (12) and (13) with respect to $q(\mathbf{S})$ and $q(\boldsymbol{\alpha})$, respectively. The VCG estimate $\hat{\mathbf{S}}$ can subsequently be determined from

$$\hat{\mathbf{S}}_{\mathrm{PTV}} = \mathbf{D}^{\dagger}\mathbf{U} \quad (18)$$

with $\mathbf{D}^{\dagger}$ the Moore–Penrose pseudoinverse of $\mathbf{D}$ and $\mathbf{U}$ an $[N\times T]$ matrix with rows $\vec{\nu}_i$.

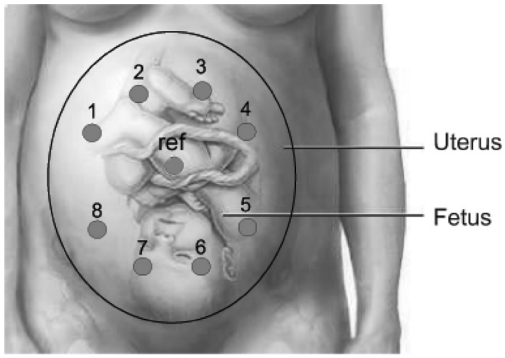

Fig. 2. Electrode positions for recording the fetal ECG and VCG from the maternal abdomen. This figure has been adopted from [31].

IV. Data Acquisition and Evaluation

To evaluate both VCG methods, the 12-lead ECG from adult patients and the fetal ECG are used. The approach used to evaluate both methods is discussed in more detail shortly (see Section IV-B).

To model the VCG of nonstandard adult patients, the 12 ECG signals from the 12-lead ECG are randomly scaled. When dealing with real recordings of such patients this scaling is expected not to be random. In fact, electrodes close to one another are expected to exhibit similar scaling parameters. However, with a random scaling being an even more challenging test, this approach suffices for evaluation of the PTV and Dower method. To minimize the effect of the randomized scaling factor generation, the final results are averaged over all heartbeats. The scaled 12-lead ECG, the original 12-lead ECG itself, and the fetal ECG acquisition are discussed in more detail shortly.

A. Data Acquisition

1) Twelve-Lead Adult ECG: The most widely used clinical ECG system is the 12-lead ECG system, consisting of the leads: I, II, III, aV_R, aV_L, aV_F, V_1, V_2, V_3, V_4, V_5, and V_6 [27].

The 12-lead ECG recordings used in this paper are taken from the MIT/BIH PTB diagnostic ECG database [28]. Next to the 12-lead ECG signals, this database also contains the corresponding Frank XYZ signals. The Frank XYZ lead system is a system comprising three orthogonal leads that, due to this orthogonality, fully describe the three dimensions of the VCG [29]. The Frank XYZ signals can, therefore, be used to evaluate the predicting performance of both the PTV and Dower methods.

A total of ten recordings is used from the database (patients 104, 105, 116, 117, 121, 122, 235, 242, 263, and 264) with a total number of 693 heartbeats. All recordings are 60-s-long and all patients are healthy.

2) Fetal ECG: As mentioned previously, the fetal ECG can be recorded from the maternal abdomen. In this paper, the fetal ECG is recorded from a single patient of 24 weeks of gestation, using the electrode configuration of Fig. 2. The total length of the signal is over 300 s and it contains more than 800 fetal heartbeats. For this gestational age of 24 weeks, the fetus is not yet covered by the isolating vernix caseosa and hence, the conduction of fetal ECG signals towards the maternal abdominal surface can be assumed uniform [14], [15].

The signals acquired from the maternal abdomen, at a sampling rate of 1 kHz, contain a mixture of fetal ECG, maternal ECG, muscular activity and other interferences. The fetal ECG is extracted from this mixture using filtering and a dynamic template subtraction method [30]. The electrode positions on the maternal abdomen with respect to one another are estimated by positioning the electrodes as accurately as possible in the configuration of Fig. 2 and estimating the shape/rounding of the abdomen.

The electrode configuration of Fig. 2 is designed in such a way that all electrodes are relatively close to the fetal heart. As this configuration is different from the electrode configuration used for the 12-lead ECG [5], the numerical description of the Dower matrix $\mathbf{D}$ cannot be used to determine the fetal VCG. Therefore, for estimation of the fetal VCG, the matrix $\mathbf{D}$ only contains the electrode positions and does not account for boundary effects and tissue inhomogeneities.

B. Evaluation of Methods

As mentioned previously, both the PTV and Dower methods are evaluated by assessing the performance of both methods in predicting ECG signals. This entails the projection of the VCG onto ECG lead vectors $\vec{D}_j$ of which the corresponding signals $\vec{V}_j$ are not included in the estimation of the VCG. These excluded ECG signals are the signals from the previously mentioned Frank XYZ system, but also signals from the 12-lead ECG that are just not used in the calculation of the VCG and that are randomly selected. The reason for not using all of the 12-lead ECG signals is to also assess the sensitivity of both VCG methods to the number of electrodes. It has to be noted here, that for the estimation of the VCG a minimum number of three ECG signals is required at all times. Again, the performance of both methods is described by means of the resemblance between the ECG signals resulting from projection of the VCG and the actually recorded ECG signal.

The resemblance between projected and recorded ECG signals is expressed quantitatively by means of ϵ, the normalized MSE between the recorded ECG signal and the VCG projection

$$\epsilon_{\mathrm{PTV}} = \frac{1}{N}\sum_{i=1}^{N} \frac{(\vec{V}_i - \hat{\alpha}_i \vec{D}_i \hat{\mathbf{S}}_{\mathrm{PTV}})(\vec{V}_i - \hat{\alpha}_i \vec{D}_i \hat{\mathbf{S}}_{\mathrm{PTV}})^T}{\vec{V}_i \vec{V}_i^T} \quad (19)$$

$$\epsilon_{\mathrm{Dower}} = \frac{1}{N}\sum_{i=1}^{N} \frac{(\vec{V}_i - \vec{\mathcal{D}}_i \hat{\mathbf{S}}_{\mathrm{Dower}})(\vec{V}_i - \vec{\mathcal{D}}_i \hat{\mathbf{S}}_{\mathrm{Dower}})^T}{\vec{V}_i \vec{V}_i^T}. \quad (20)$$

As mentioned previously in Section I, on average about 83% (i.e., approximately the mean between 70 and 95%) of the power of the ECG signals can be predicted by projection of the VCG. Consequently, MSE values of about -7.5 dB, i.e., 17%, signify a relatively accurate VCG, i.e., MSE values larger than about -7.5 dB indicate that, besides imperfections in the dipole model, additional inaccuracies in the VCG methods have to be present as well.

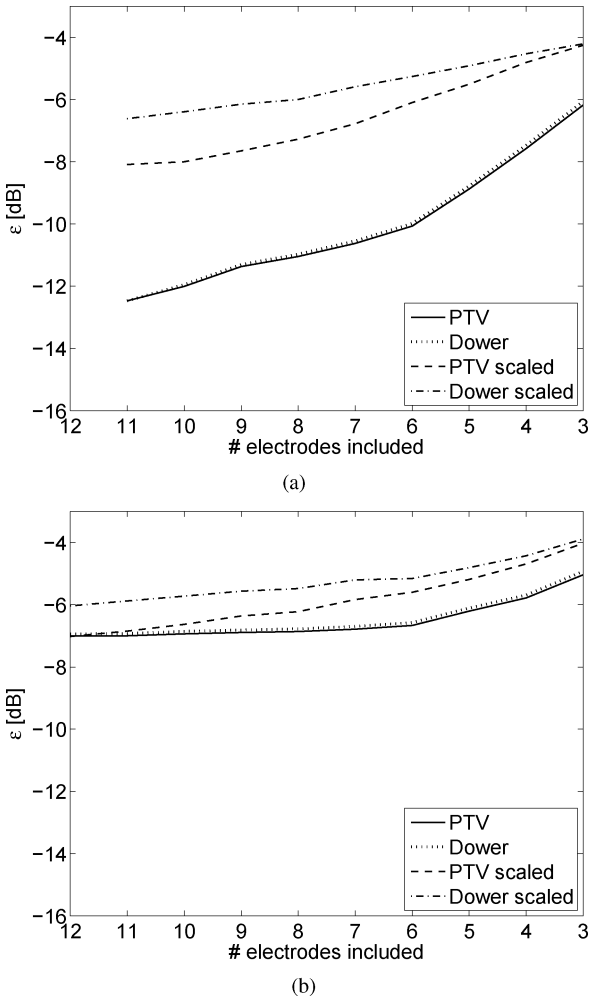

Fig. 3. Normalized MSE ϵ between the ECG signals determined from projection of the VCG and the recorded ECG signals. The MSE ϵ is determined for both the PTV method and the Dower method for both scaled and unscaled ECG signals. (a) VCG projections are compared to the omitted ECG signals. (b) VCG projections are compared to the Frank XYZ leads. Note that in both graphs, for the unscaled ECG signals, the values for ϵ for both methods are practically on top of one another.

The fetal VCG determined from real fetal ECG signals cannot be validated with respect to Frank XYZ signals. Therefore, the performance of both VCG methods is only evaluated by calculating the fetal VCG with less than the eight electrodes, as depicted in Fig. 2, and subsequently comparing VCG projections to the omitted ECG signals. The performance is again expressed quantitatively by means of ϵ.

Finally, for both the adult 12-lead ECG and the fetal ECG recordings, the variance $\mathbf{\Sigma}$ is determined by assessing, for each individual ECG complex, the variance of the signal that is obtained by subtracting a template ECG complex from the recorded ECG complexes. This template ECG complex is generated by averaging all ECG complexes within each signal.

V. Results

A. Twelve-Lead ECG

In Fig. 3, the MSE ϵ is depicted for both the PTV method and the Dower method.

Fig. 3(a) and (b) shows ϵ for the predictive performance of the VCG with respect to omitted electrodes and Frank XYZ leads, respectively. The values of ϵ are determined as a function of the number of ECG signals included. As mentioned previously, the signals that are omitted (i.e., horizontal axis values larger than zero) are randomly selected and the depicted values represent the mean values across all the heartbeats for all of the patients.

From Fig. 3, it can be seen that the performance of both methods is approximately the same for unscaled ECG signals, with the developed method performing marginally better. Since the Dower method has been developed for these recordings, not much improvement would have been expected here though. It is, however, striking that even for small numbers of electrodes included, the VCG determined with the Dower method still is as accurate as a method that can, to some extent, account for interpatient differences in signal propagation. The most probable reason for this is that the inaccuracy in the Dower method, also for few electrodes included, is smaller than the error originating from nondipolar effects (see Section IV-A). This argumentation is confirmed by the fact that all values for ϵ, except the ones for only three or four electrodes included, are smaller than -7.5 dB, indicating a relatively accurate VCG estimation. For the scaled ECG signals, the developed PTV method significantly outperforms the Dower method with MSE values below -7.5 dB in most situations.

From these figures, it can also be seen that the variational inference only approximates the MAP solution for $\mathbf{S}$ in (9), namely, in case the variational inference method would generate the true MAP solution, the PTV values for ϵ between scaled and unscaled ECG signals would nearly be the same.

In addition, from Fig. 3(a) and (b), it can be seen that, for the modeled nonstandard patients (and thus, scaled signals), for the PTV method the number of included electrodes larger than the minimally required number of three electrodes can be halved with respect to the Dower method in order to still obtain similar ϵ values. This can result in more patient-friendly, comfortable ECG measurements as fewer electrodes need to be positioned on the patient's skin.

Although the difference in performance between the PTV method and the Dower method for scaled ECG signals appears to be small in Fig. 3(b), it yields a significant difference in the VCG estimates of Fig. 4. More precisely, because the Frank XYZ leads together comprise the VCG, comparing the VCGs of both methods to one another gives some insight into how this small difference in MSE ϵ translates to actual VCG estimates. Fig. 4 indicates that the nonstandard patients' VCG estimated by the PTV method resembles the VCG determined from unscaled ECG signals significantly better than the VCG estimated by the Dower method. Here, the unscaled VCG serves as reference for the VCGs determined from the scaled signals. The significance in this difference lies in the fact that some ECG applications call for comparison of two or more vectorcardiographic loops, serial ECG analysis probably being the most notable [32]. Such comparisons can be considerably affected by slight interrecording changes in the VCG. For instance, a small Q-wave in a projected ECG complex may completely vanish in the consecutive

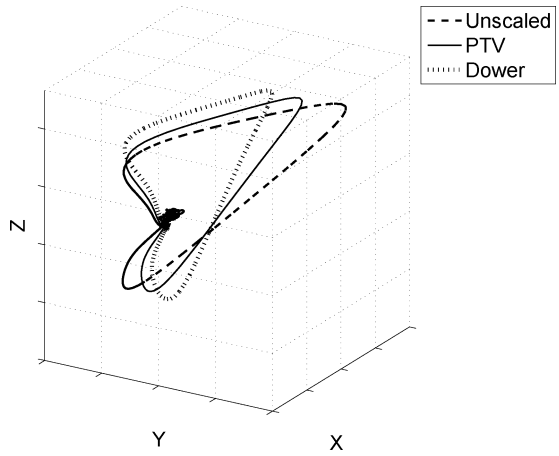

Fig. 4. VCG determined from scaled ECG recordings with the developed PTV method and with the conventional Dower method. For reference, also the corresponding VCG from the unscaled ECG recordings is depicted.

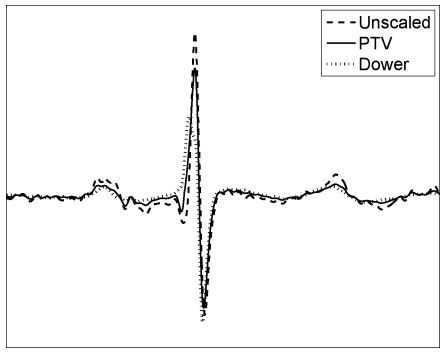

Fig. 5. Projections of the VCGs of Fig. 4 onto the normalized lead vector (0, 0.96, −0.27). In contrast to the ECG determined by the PTV method and the unscaled reference ECG, in the ECG determined by the Dower method the Q-wave is absent.

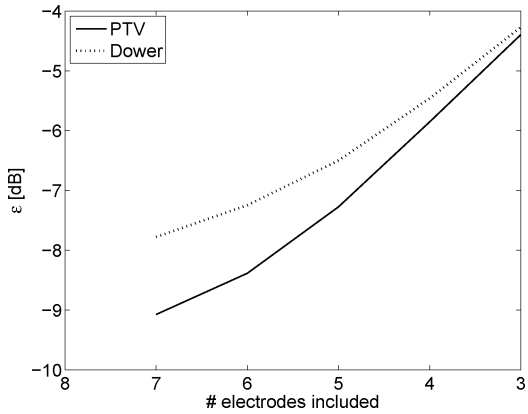

Fig. 6. Normalized MSE ϵ between the fetal ECG signals determined from projection of the fetal VCG and the fetal ECG signals that are omitted from the calculation of the VCG. The MSE ϵ is determined for both the PTV method and the Dower method.

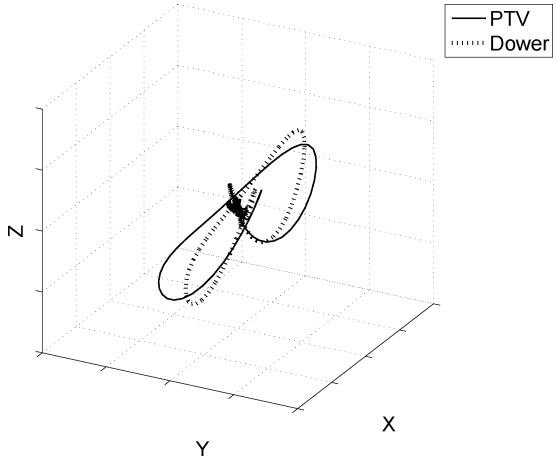

Fig. 7. Fetal VCG determined with both the PTV method and the conventional method.

complex. This is illustrated in Fig. 5, in which the VCGs of Fig. 4 are projected onto a specific lead vector. Notwithstanding this improved performance of the PTV method with respect to the Dower method, the PTV method also suffers from inaccuracies, as can be seen from the difference between the unscaled VCG and the VCG estimated by the PTV method in Fig. 4. These inaccuracies are mostly due to approximations made by the variational inference and the fact that attenuation effects are assumed isotropic, i.e., the ratios between elements within each row of $\mathbf{D}$ are kept fixed.

B. Fetal ECG

In Fig. 6, the MSE ϵ is depicted for the VCG determined from actually recorded fetal ECG signals.

From Fig. 6, it can be seen that also for ECG signals with a lower SNR, the developed PTV method outperforms the Dower method. The difference between both methods is illustrated once more in Fig. 7 in which the fetal VCG determined with both methods is depicted.

The difference between both VCGs can, according to the model of (3), be explained by the different attenuation effects on the ECG signals recorded with different electrodes.

VI. Discussion and Conclusion

The presented method outperforms the currently existing method for VCG determination in all situations, although the difference between both methods for patients with standard body composition and geometry is negligible. For patients that do not conform to the standard, such as fetuses, however, the performance of the developed method appears to be significantly better than the performance of the conventional method.

Notwithstanding this improvement in VCG determination, the developed method is liable to inaccuracies since the applied variational inference method only approximates the MAP solution. By extending this method with other probability distributions, instead of just the Gaussian, performance of this method can be improved, however, potentially leading to a computational higher complexity, e.g., due to required numerical evaluation instead of analytical evaluation as is the case with the

Gaussian distribution. At this moment, for both scaled and unscaled ECG recordings, the PTV method requires, on average, less than five iterations to converge to a stationary solution, yielding a relatively small computational load.

Other ways of improving the developed method are the inclusion of prior information on the scaling parameters $\boldsymbol{\alpha}$, more precisely determined electrode positions, and the extension of the dipole model to enable it to also deal with nondipolar components. For the latter, an overview of ways to extend the dipole model is provided in [33], including the addition of another dipole and the use of multipoles. More recent extensions of the dipole model include the use of distributed source models, as discussed in [34]. Including prior information on $\boldsymbol{\alpha}$ implies the inclusion of prior information on spatial information, i.e., the heart–electrode distances, as well [35]. Following the principle of maximum entropy [23] to determine the appropriate corresponding prior probability distribution and including this distribution in (9) would result in an analytically unsolvable expression for the posterior probability distribution. In turn, this would require the use of computationally more complex numerical approaches to infer the MAP solution. The extension of the dipole model would also lead to computational more complex numerical approaches. Although all these improvements are expected to lead to a more accurate VCG estimation, this increased accuracy is expected to be overshadowed by the inaccuracies caused by nondipolar contributions in the ECG, as described in the first paragraph of Section I, with the exception of improvements in the variational inference and the extension of the model. Hence, the proposed improvements to the developed method are expected to cause higher computational complexity (improved variational inference, prior information on $\boldsymbol{\alpha}$, and extension of the model) and yield more laborious measurements (more precise electrode positions), while the benefits of most improvements are negligible. In addition, a higher computational complexity prevents the use of the PTV method in real-time applications.

For development of the PTV method, several assumptions have been made, including the Gaussian distribution of the noise and mutual independence of the scaling parameters $\boldsymbol{\alpha}$. The assumption of the noise having a zero-mean Gaussian distribution is adopted from the inverse Dower matrix method. In this method, inaccuracies in the dipole model regarding boundary effects, tissue inhomogeneities, and nondipolar components are assumed to be accounted for by the numerical description of the Dower matrix. Although this assumption is not completely valid, resulting in reduced accuracy in VCG estimation, the method is reported to perform sufficiently well to support clinical decision making [12]. With the PTV method outperforming the inverse Dower matrix method, the PTV method is expected to also perform sufficiently well for clinical decision making. This, however, remains to be demonstrated in clinical practice. The mathematical benefits of the Gaussian-noise assumption, yielding the final algorithm analytically solvable, can, therefore, be considered of larger interest than the modeling error it provokes. The assumption of the scaling parameters $\boldsymbol{\alpha}$ being mutually independent is, in contrast to other statistical independencies, not justified by applying d-separation. In fact, both this assumption of independence and the assumption of a uniform prior for $\boldsymbol{\alpha}$ are inaccurate and result in decreased performance of the PTV method. These assumptions are nevertheless needed for the sake of tractability. However, even with these inaccurate assumptions, the results in Figs. 3 and 6 show that the PTV method outperforms the Dower method. Including prior information on $\boldsymbol{\alpha}$ is nevertheless expected to lead to substantially improved performance of the PTV method.

The normalized MSE ϵ in predicting ECG signals from the VCG is, for the unscaled ECG recordings, smaller than -10 dB for VCGs determined from six included electrodes or more. Although this error can be fully attributed to nondipolar components in the precordial ECG leads, part of this error should be attributed to inaccuracies in the linearization of boundary effects and tissue inhomogeneities as well. Here, the main inaccuracy is caused by the assumption of the scaling $\boldsymbol{\alpha}$ being isotropic, and hence, the assumption of the ratio between the elements within each row of $\mathbf{D}$ being fixed. For scaled ECG signals and the fetal ECG, besides model inaccuracies also the approximation in the variational inference and decreased signal to noise ratios (for the fetal ECG) give rise to increased MSE. Based on the differences between scaled and unscaled PTV results in Fig. 3 (as discussed in Section V-A), this increase in ϵ due to variational inference can be up to 5 dB.

From Figs. 3 and 6, it can be seen that the PTV method requires less ECG signals than the Dower method to obtain similar MSE values in the prediction of reference ECG signals. Consequently, the use of the PTV method in ambulatory ECG monitoring is expected to decrease patient discomfort and reduce bandwidth requirements for wireless data transmission.

Notwithstanding the inaccuracies mentioned previously, the developed method provides a way for estimating a VCG, tailored to each specific patient. For patients conforming to the standard, the improvement with respect to the conventional method is negligible, but for nonstandard patients the improvement is significant. On the one hand, the VCG can be determined with increased accuracy, which for the fetus may result in improved early-stage diagnosis and perhaps even treatment of congenital heart diseases, whereas, on the other hand, for adult patients it can result in a smaller number of required electrodes, improving patient comfort and facilitating ambulatory monitoring applications.

Additionally, since the method also estimates $\boldsymbol{\alpha}$ in (9), for the fetal VCG, the method can be used in future to estimate the position of the fetal heart with respect to the electrodes—requiring assumptions on tissue homogeneity—and hence, the position of the fetus inside the uterus. In addition, the estimation of $\boldsymbol{\alpha}$ might in future be used to estimate distributed electrical activity of the heart. Furthermore, because of the similar nature of the problem in fetal magnetocardiography [36], the method may also be applied on fetal magnetocardiogram (MCG) signals. With regard to fetal ECG/MCG monitoring, the capability of the method to predict the morphology of fetal ECG/MCG signals that cannot be recorded directly can have significant value in clinical practice, e.g., through determination of the 12-lead ECG/MCG. This prediction of the 12-lead ECG and its use in clinical practice is, therefore, a possible subject of further studies as well.

REFERENCES

[1] D. Geselowitz, "Dipole theory in electrocardiography," *Amer. J. Cardiol.*, vol. 14, no. 9, pp. 301–306, 1964.

[2] H. Burger and J. van Milaan, "Heart-vector and leads," *Br. Heart J.*, vol. 8, no. 3, pp. 157–161, Jul. 1946.

[3] L. Horan, N. Flowers, and D. Brody, "Principal factor waveforms of the thoracic QRS complex," *Circ. Res.*, vol. 15, pp. 131–145, 1964.

[4] L. Horan, N. Flowers, and C. Miller, "A rapid assay of dipolar and extradipolar content in the human electrocardiogram," *J. Electrocardiol.*, vol. 5, no. 3, pp. 211–224, 1972.

[5] J. Malmivuo and R. Plonsey, *Bioelectromagnetism—Principles and Applications of Bioelectric and Biomagnetic Fields*. New York: Oxford Univ. Press, 1995.

[6] D. Gabor and C. Nelsen, "Determination of the resultant dipole of the heart from measurements on the body surface," *J. Appl. Phys.*, vol. 25, no. 4, pp. 413–416, Apr. 1954.

[7] R. Gulrajani, F. Roberge, and P. Savard, "Moving dipole inverse ECG and EEG solutions," *IEEE Trans. Biomed. Eng.*, vol. BME-31, no. 12, pp. 903–910, Dec. 1984.

[8] F. Greensite and G. Huiskamp, "An improved method for estimating epicardial potentials from the body surface," *IEEE Trans. Biomed. Eng.*, vol. 45, no. 1, pp. 98–104, Jan. 1998.

[9] B. He and D. Wu, "Imaging and visualization of 3-D cardiac electric activity," *IEEE Trans. Inf. Technol. Biomed.*, vol. 5, no. 3, pp. 181–186, Sep. 2001.

[10] R. Hoekema, G. Uijen, and A. van Oosterom, "On selecting a body surface mapping procedure," *J. Electrocardiol.*, vol. 32, no. 2, pp. 93–101, 1999.

[11] L. Edenbrandt and O. Pahlm, "Vectorcardiogram synthesized from a 12-lead ECG: Superiority of the inverse Dower matrix," *J. Electrocardiol.*, vol. 21, no. 4, pp. 361–367, 1988.

[12] G. Dower, H. Machada, and J. Osborne, "On deriving the electrocardiogram from vectorcardiographic leads," *Clin. Cardiol.*, vol. 3, pp. 87–95, 1980.

[13] S. Kenchaiah, J. Evans, D. Levy, P. Wilson, E. Benjamin, M. Larson, W. Kannel, and R. Vasan, "Obesity and the risk of heart failure," *New Engl. J. Med.*, vol. 347, no. 5, pp. 305–313, Aug. 2002.

[14] J. Oldenburg and M. Macklin, "Changes in the conduction of the fetal electrocardiogram to the maternal abdominal surface during gestation," *Amer. J. Obstet. Gynecol.*, vol. 129, no. 4, pp. 425–433, Oct. 1977.

[15] T. Oostendorp, "Modelling the foetal ECG," Ph.D. dissertation, K. U. Nijmegen, Nijmegen, The Netherlands, 1989.

[16] R. Vullings, C. Peters, M. Mischi, S. Oei, and J. Bergmans, "Fetal movement quantification by fetal vectorcardiography: A preliminary study," in *Proc. IEEE EMBC*, 2008, pp. 1056–1059.

[17] K. Greene, G. Dawes, H. Lilja, and K. Rosén, "Changes in the ST waveform of the fetal lamb electrocardiogram with hypoxemia," *Amer. J. Obstet. Gynecol.*, vol. 144, pp. 950–958, Dec. 1982.

[18] A. Camm, T. Lüscher, and P. Serruys, *The ESC Textbook of Cardiovascular Medicine*. Oxford, U.K.: Blackwell, 2006.

[19] C. Bishop, *Pattern Recognition and Machine Learning*. New York: Springer Science+Business Media LLC, 2006.

[20] E. Moore, "On the reciprocal of the general algebraic matrix," *Bull. Amer. Math Soc.*, vol. 26, pp. 394–395, 1920.

[21] R. Penrose, "A generalized inverse for matrices," *Proc. Cambridge Philos. Soc.*, vol. 51, pp. 406–413, 1955.

[22] E. Jaynes, *Probability Theory: The Logic of Science*. Cambridge, U.K.: Cambridge Univ. Press, 2003.

[23] K. Knuth, "Bayesian source separation and localization," in *Proc. SPIE 1998 Bayesian Inference Inverse Problems*, San Diego, CA, Jul. 1998, vol. 3459, pp. 147–158.

[24] R. Barr, M. Ramsey, and M. Spach, "Relating epicardial to body surface potential distributions by means of transfer coefficients based on geometry measurements," *IEEE Trans. Biomed. Eng.*, vol. BME-24, no. 1, pp. 1–11, Jan. 1977.

[25] Y. Yamashita and T. Takahashi, "Use of the finite element method to determine epicardial from body surface potentials under a realistic torso model," *IEEE Trans. Biomed. Eng.*, vol. BME-31, no. 9, pp. 611–621, Sep. 1984.

[26] G. Parisi, *Statistical Field Theory*. Jackson, TN: Perseus Books Publ. LLC, 1988.

[27] A. Guyton and J. Hall, *Textbook of Medical Physiology*, 10th ed. Philadelphia, PA: Saunders, 2000.

[28] MIT/BIH PTB diagnostic ECG database. (1999). [Online]. Available: http://www.physionet.org/physiobank/database/ptbdb/

[29] E. Frank, "An accurate, clinically practical system for spatial vectorcardiography," *Circulation*, vol. 13, pp. 737–749, 1956.

[30] R. Vullings, C. Peters, R. Sluijter, M. Mischi, S. Oei, and J. Bergmans, "Dynamic segmentation and linear prediction for maternal ECG removal in antenatal abdominal recordings," *Physiol. Meas.*, vol. 30, pp. 291–307, 2009.

[31] C. Rabotti, M. Mischi, J. van Laar, S. Oei, and J. Bergmans, "Estimation of internal uterine pressure by joint amplitude and frequency analysis of electrohysterographic signals," *Physiol. Meas.*, vol. 29, pp. 829–841, 2008.

[32] L. Sörnmo, "Vectorcardiographic loop alignment and morphologic beat-to-beat variability," *IEEE Trans. Biomed. Eng.*, vol. 45, no. 12, pp. 1401–1413, Dec. 1998.

[33] D. Geselowitz, "On the theory of the electrocardiogram," *Proc IEEE*, vol. 77, no. 6, pp. 857–876, Jun. 1989.

[34] Z. Liu, C. Liu, and B. He, "Noninvasive reconstruction of three-dimensional ventricular activation sequence from the inverse solution of distributed equivalent current density," *IEEE Trans. Med. Imag.*, vol. 25, no. 10, pp. 1307–1318, Oct. 2006.

[35] W. Penny, N. Trujillo-Barreto, and K. Friston, "Bayesian fMRI time series analysis with spatial priors," *NeuroImage*, vol. 24, no. 2, pp. 350–362, 2005.

[36] M. Popescu, E.-A. Popescu, K. Fitzgerald-Gustafson, W. Drake, and J. Levine, "Reconstruction of fetal cardiac vectors from multichannel fMCG data using recursively applied and projected multiple signal classification," *IEEE Trans. Biomed. Eng.*, vol. 53, no. 12, pp. 2564–2576, Dec. 2006.

Rik Vullings was born in Venray, The Netherlands, in 1980. He received the M.Sc. degree in applied physics (*cum laude*) in 2005 from the Eindhoven University of Technology, Eindhoven, The Netherlands, where he is currently working toward the Ph.D. degree with the Department of Electrical Engineering.

His current research interests include signal processing with applications in fetal monitoring.

Chris H. L. Peters was born in Sittard, The Netherlands, in 1977. He received the M.Sc. degree in applied physics in 2001 and the P.D.Eng. degree in 2006 from the Eindhoven University of Technology, Eindhoven, The Netherlands, where he is currently working toward the Ph.D. degree in applied physics.

He is currently a Medical Physicist with the Amphia Hospital, Breda, The Netherlands, where he is the Head of the Department of Medical Technology.

Iman Mossavat was born in Mashhad, Iran, on June 27, 1979. He received the B.S. degree from the Department of Electrical Engineering, Ferdowsi University of Mashhad, Mashhad, Iran, in 2002, the M.Sc. degree from the Department of Electrical Engineering, Sharif University of Technology, Tehran, Iran, in 2005, and the Master's of Engineering degree from the Department of Electrical and Computer Engineering, National University of Singapore, Singapore, in 2008. He is currently working toward the Ph.D. degree in electrical engineering with the Eindhoven University of Technology, Eindhoven, The Netherlands.

His current research interests include signal processing and Bayesian machine learning.

S. Guid Oei received the Ph.D. degree from Leiden University, Leiden, The Netherlands, in 1996.

He is currently a Gynaecologist–Perinatologist with Máxima Medical Center (MMC), Veldhoven, the Netherlands. He is also a Professor of fundamental perinatology with the Department of Electrical Engineering Eindhoven University of Technology, Eindhoven, the Netherlands. He subspecialized in perinatology at Flinders University, Adelaide, S.A., Australia. Since 2005, he has been the Dean of the MMC Academy and the Director of the Medical Simulation and Education Centre.

Jan W. M. Bergmans (M'85–SM'91) received the Elektrotechnisch Ingenieur (*cum laude*) degree and the Ph.D. degree from Eindhoven University of Technology, Eindhoven, The Netherlands, in 1982 and 1987, respectively.

From 1982 to 1999, he was with Philips Research Laboratories, Eindhoven, where he was engaged in signal-processing techniques and IC architectures for digital transmission and recording systems. In 1988 and 1989, he was an Exchange Researcher with Hitachi Central Research Laboratories, Tokyo, Japan. Since 1999, he has been a Professor and the Chairman of the Signal Processing Systems Group, Eindhoven University of Technology, and an Advisor with Philips Research. He has authored or coauthored extensively in refereed journals, has authored a book *Digital Baseband Transmission and Recording* (Kluwer Academic Publishers, 1996), and holds around 40 U.S. patents.